ADVANCED MATERIALS
www.advmat.de

Programmable Multicolor Room-Temperature Phosphorescence Hydrogels via the Synergy of Freeze-Soaking and Salting-Out

Muqing Si, Weihao Feng, Depeng Liu, Wen Hong, Chi Chen, Adam Hernandez, Yat Him Cyrus Wong, Xiaobing Zuo, Hua Zhou, Wei Lu, Tao Chen,* and Ximin He**

Room temperature phosphorescence (RTP) is rarely achieved in hydrogel systems, as water severely quenches their emission. Achieving multicolor RTP in hydrogels is even more challenging, despite its high potential in cutting-edge applications such as advanced anti-counterfeiting and camouflaging skins. Here, a universal strategy is presented to fabricate multicolor RTP hydrogels through the cascading freeze-soaking and salting-out process (F-S method). This method induces in situ polymer assembly around the phosphors, providing effective confinement and protection against quenching. As a result, RTP hydrogel (RTPgel) with strong phosphorescence (lifetime > 200 ms and afterglow >10 s), high water content (71 %), and excellent flexibility (stretchability > 3000%) is achieved in a modal system composed of polycyclic aromatic boronic acids (PABAs)-grafted polyvinyl alcohol (PVA). Since chain aggregation strongly correlates with the kosmotropic nature of the salt solution, the phosphorescence properties, including lifetime and intensity, are feasibly tunable by re-soaking the hydrogels in solution with different types of salts or concentrations, enabling programmable spatiotemporal emission patterns. Such a method is universal, adaptable for various luminophores and polymer matrices, allowing customizable emission colors across a wide spectrum. Moreover, it is compatible with scalable, high-precision fabrication techniques such as fiber spinning, direct ink writing (DIW), and digital light processing (DLP) 3D printing.

1. Introduction

Room temperature phosphorescent (RTP) materials, featuring long afterglow and large Stokes shifting in moderate environments, have drawn significant attention in the past decade due to their promising prospect in several cutting-edge applications, including bio-imaging, anti-counterfeiting, indicating, and sensing.[1–7] Polymeric RTP materials have been elaborately investigated because of their feasibility for fabrication, low cost, and lightweight.[8,9] In this context, elegant strategies have been successfully applied for achieving polymeric RTP material, including host-guest interaction,[10–13] H-aggregation,[14,15] clusterization,[16,17] crystallization,[18–21] and metal-organic frameworks.[22–24] To summarize, suppressing the molecular motion for obliterating the nonradiative decay by trapping the phosphor in a dry and rigid matrix is the main merit of building polymeric RTP materials[25–28](**Figure 1A**). In this context, dry-state hydrogen-bond-rich polymeric

M. Si, W. Hong, C. Chen, A. Hernandez, Y. H. C. Wong, X. He
Department of Materials Science and Engineering
University of California
Los Angeles, CA 90095, USA
E-mail: ximinhe@ucla.edu

M. Si, W. Feng, D. Liu, W. Lu, T. Chen
State Key Laboratory of Advanced Marine Materials
Zhejiang Key Laboratory of Extreme-environmental Material Surfaces and Interfaces
Ningbo Institute of Materials Technology and Engineering
Chinese Academy of Sciences
Ningbo 315201, China
E-mail: luwei@nimte.ac.cn; tao.chen@nimte.ac.cn

X. Zuo, H. Zhou
X-Ray Science Division
Argonne National Laboratory
Lemont, IL 60439, USA

M. Si, W. Feng, D. Liu, W. Lu, T. Chen
School of Chemical Sciences
University of Chinese Academy of Sciences
Beijing 100049, China

The ORCID identification number(s) for the author(s) of this article can be found under https://doi.org/10.1002/adma.202518652

DOI: 10.1002/adma.202518652

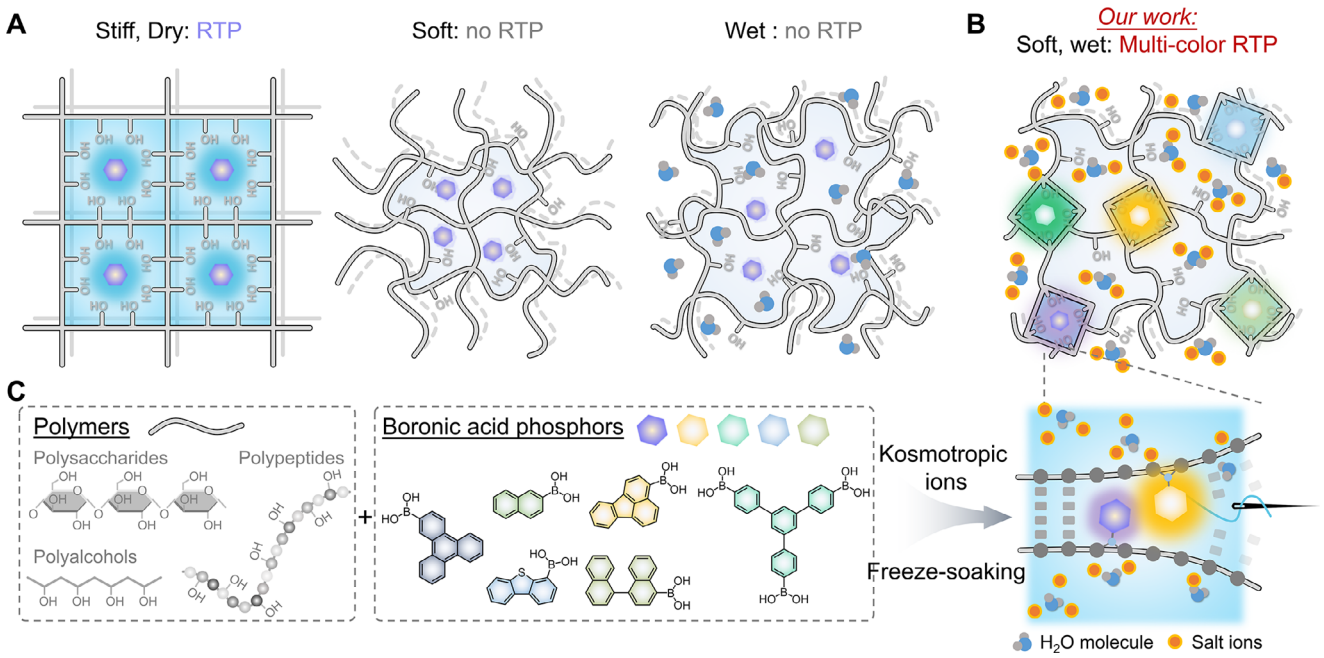

Figure 1. Strategies for fabricating polymeric RTP materials. A) Normal strategies for building RTP polymers by trapping phosphors into a rigid and dry matrix for suppressing the molecular motion. B) Wet matrix and soft matrix are unable to provoke the phosphorescence due to the drastic molecular motion of phosphor molecules and solvent molecules. C) Our strategy for building multi-color RTP hydrogels by harnessing the synergy of freeze-soaking and salting-out for sealing phosphores within interchain constraints, which has universality for various polymers, phosphors, and fabrication methods.

materials, such as polyvinyl alcohol (PVA),[29,30] poly acrylic acid (PAAc)[31] with a glass transition temperature (T_g) much higher than room temperature, are the few practical choices for an ideal RTP matrix. However, these matrices are usually highly hydroscopic, causing derived RTP materials to be highly sensitive to surrounding water molecules and easily quenched. Such features limit current RTP materials in their total dry state, with poor stretchability and flexibility. It is a challenging but urgent task to fabricate water-insensitive RTP materials, especially hydrogel-based polymeric RTP materials, which are featured by soft, wet, and compliant, making them a promising candidate for cutting-edge applications, including soft electronics, soft actuators/robotics, and in vivo imaging material.[18,32,33]

To stabilize the phosphors within highly hydrated polymer skeletons in hydrogels, it is important to confine the phosphors in a rigid and waterless micro-environment,[34] which is hardly obtainable in hydrogels. A few possible routines were proposed. Tian et al. specially designed a phosphorescence hydrogel composed of dangling cyclodextrin (CD) and a-bromonaphthalene (α-BrNp) side group.[35] The α-BrNp phosphor was isolated in CD from water molecules through host-guest interaction, which allows its phosphorescence emission of α-BrNp within the hydrogel matrix. Our recent work proved that such a strategy would work even if the CD-phosphor assembly is physically absorbed by rather than attached to the polymer network.[13] Besides doping or grafting the protected phosphors into the hydrogel matrix to build RTP hydrogels, the polar side groups of hydrogels can also emit phosphorescence if they are properly restricted. Wu et al. have proposed a crystallization-induced clusterization method to confine the polymeric matrix in a crown ethers (CE)/polyacrylamide (PAAm) composite hydrogel.[18] After polymerization of PAAm hydrogel, the solubility of CD in the mixture decreased, resulting in in situ precipitation and crystallization of CE. The CE crystals squeezed the polymer matrix, causing the carbonyl clusters and thus phosphorescence emission. A similar strategy can be found in the work from Zhao et al.[36] They synthesized a phosphorescent hydrogel by copolymerizing acrylamide (Am) with N-acryloyl-aminoundecanoic acid (NAUA). The hydrophobic NAUA induces phase separation in the hydrogel network, forming hydrophobic phases that stiffen the structure and constrain the mobility of water molecules and chain segments, triggering the RTP emission of the carboxylic acid group clusters. Similarly, poly(vinyl alcohol)/poly(calcium maleate) hydrogel prepared through a drying and rehydration process has also been proven to be phosphorescent by Wang et al.[33] Nevertheless, these methods for creating RTP hydrogels could only be achieved in particular hydrogel matrices with special chemical designs, to intentionally implant the hydrophobic microenvironment within the matrix. Moreover, these microenvironments are usually not compatible with a wide range of phosphors. Limited selection in phosphors prohibits achieving multi-color RTP hydrogels with a wide spectrum emission. It would be more inhibited to customize phosphorescent hydrogel with programmable color, intensity, and afterglow. Such monochromatic afterglow limits their utility to single-channel optical outputs, restricting applications in data encryption, complex pattern display, and multiplexed sensing. Multicolor RTP hydrogels could offer tunable and even site-specific emission, allowing a more powerful single material platform with multi-channel emission and spatiotemporal emission in a complex pattern, which would be beneficiary for cutting-edge applications such as high-level anticounterfeiting and camouflaging skin.[37–40]

Herein, we proposed a novel strategy for fabricating hydrogels with highly efficient RTP and ultralong afterglow by taking advantage of the synergy of freeze-soaking and salting-out (Figure 1B,C). This method has been demonstrated as a universal strategy to strengthen polymer-polymer associations and induce chain aggregation, ranging from semicrystalline polymers (e.g., polyvinyl alcohol,[41] polyethylene oxide[42,43]), hydrophilic polymers (e.g., polyacrylic amide,[44] poly(2-hydroxyethyl methacrylate)[45]) to biopolymers (gelatin, hyaluronic acid[46]). Specifically, freeze-soaking and salting-out is a method to fabricate hydrogels by soaking the frozen polymer precursor in salting-out aqueous solutions, and has been widely leveraged to produce tough hydrogels by us and others.[41,47,48] According to the Hofmeister effect, aqueous solutions of kosmotropic salts, such as sodium citrate (Na_3Cit), sodium sulfate (Na_2SO_4), and sodium carbonate (Na_2CO_3), etc., are capable of driving polymer chains assembled into aggregates.[43] Based on this principle, we hypothesize that the synergy of freeze-soaking and salting-out method can efficiently provoke chain aggregates to embed and stabilize the grafted phosphors in the aqueous enviornment, resulting in RTP hydrogels. As a primary demonstration, the polycyclic aromatic boronic acids (PABAs) are grafted onto the polyvinyl alcohol (PVA) chain by ultrasound-synchronized B-O-click reaction. The as-prepared PABA@PVA precursor was processed by the freeze-soak strategy to get PABA@PVA RTP hydrogel (RTPgel). Benefiting from the synergy of freeze-soak and salting out, PABA phosphors can be successfully stabilized inside the PVA microcrystals and protected from water molecules. As a result, PABA@PVA RTP hydrogel demonstrated a long lifetime of 236 ms and afterglow more than 10 s, while remaining highly hydrated (hydration ratio ≈77%), flexible, and stretchable. Compared with existing strategies that rely on specially designed matrices or hydrophobic microdomains, the freeze-soaking/salting-out synergy offers a general and chemistry-independent route to stabilize phosphors within a fully hydrated network. The simplicity and universality of this method allow broad phosphor compatibility and scalable fabrication across multiple processing platforms. Thus, full-spectrum multicolor afterglow can be achieved by carefully selecting the PABA phosphors or incorporating commercial dyes into the hydrogels by doping. As a universal method for fabricating phosphorescent hydrogels, such a method could also be adopted for developing natural polymer-based phosphorescent hydrogels. The feasibility of such a method was further evidenced by customizable shaping through molding, extrusion, and 3D printing.

2. Result

2.1. Fabrication of RTPgel

RTP hydrogels can be readily prepared from a precursor composed of phosphor-grafted PVA (M_w ≈89,000 g/mol) using a reported freeze-soak and salting out (F-S) procedure (**Figure 2A**). Starting from phosphor triphenylene-2-ylboronic acid (2TPBA), the precursor is synthesized by grafting 2TPBA onto the PVA chains via a sonication-triggered B-O click reaction at 80 °C.[49] The resulting precursor solution is poured into a mold, frozen at −20 °C, and subsequently thawed in 2 M sodium citrate (Na_3Cit) solution at room temperature to yield the 2TPBA@PVA RTPgel (Figure S1, Supporting Information).[47] In this article, RTPgel is used to denote the 2TPBA@PVA RTP hydrogel unless otherwise stated. As shown in Figure 2B, the resulting RTPgel is highly stretchable and flexible, capable of undergoing large deformations such as folding, rolling, and twisting without any noticeable change in its phosphorescent properties. Tensile testing revealed that the gel can be stretched over 3000% of its original length, confirming its remarkable flexibility (Figure 2C). Figure 2D,E presents the photoluminescence (PL) and phosphorescence (Phos.) spectra (delay time = 0.5 ms) of the RTPgel. Two emission bands appear at 393 and 470 nm in the PL spectrum, while only the 470 nm band remains in the phosphorescence spectrum. Lifetime measurements confirm that the 393 nm peak corresponds to fluorescence with a lifetime of 2.3 ns, and the 470 nm peak corresponds to phosphorescence with a lifetime of 236 ms (Figure S2, Supporting Information).

The fabrication process was further optimized to enhance phosphorescent performance. The freezing temperature (T_{freeze}) was set at −20 °C as it can quickly freeze the precursor when generating RTPgels with better phosphorescence performance compared to lower T_{freeze} (Figure S3, Supporting Information). The optimal reaction time was determined to be 3 h, whose precursor yielded the brightest fluorescence emission (Figure S4, Supporting Information). The ideal phosphor content was found to be 1 wt% (relative to PVA), producing RTPgels with strongest phosphorescence and longest lifetime (Figure S5, Movie S1, Supporting Information). Excess phosphor beyond 1 wt% resulted in unreacted residues in the precursor, potentially quenching phosphorescence via inter-phosphor energy transfer. The solid content of the precursor also has a significant influence on the phosphorescence performance of the resultant hydrogel. Increasing the solid content of the precursor enhanced both phosphorescence intensity and lifetime (Figure S6, Movie S2, Supporting Information). The influence of molecular weight (M_w) was also detailed, showing that PVA with longer chains is more advantageous in creating RTPgels with better phosphorescence performance (Figure S7, Movie S3, Supporting Information). The RTPgels also demonstrated excellent phosphorescence stability over mechanical deformation and UV aging (Figures S8 and S9, Supporting Information).

2.2. Origin of Room-Temperature Phosphorescence

Phosphorescence typically arises when the molecular motion of the phosphor and the surrounding matrix is significantly restricted.[50–53] Regarding the obtained RTPgel, we propose a hydrophobic assembly-induced in situ crystallization mechanism to explain the enhanced phosphorescence resulting from the synergy of freeze-thawing and salting-out. First, upon grafting the highly hydrophobic aromatic molecule 2TPBA onto hydrophilic PVA chains dissolved in water, 2TPBA autonomously undergoes J-aggregation driven by hydrophobic interactions. This is evidenced by a red shift in the main absorption peak of 2TPBA in water compared to that in DMSO (Figure S10A, Supporting Information).[54] Macroscopically, this aggregation leads to a transition of the PVA solution from transparent to opaque (Figure S10B, Supporting Information), further confirming the formation of interchain hydrophobic associations. At the

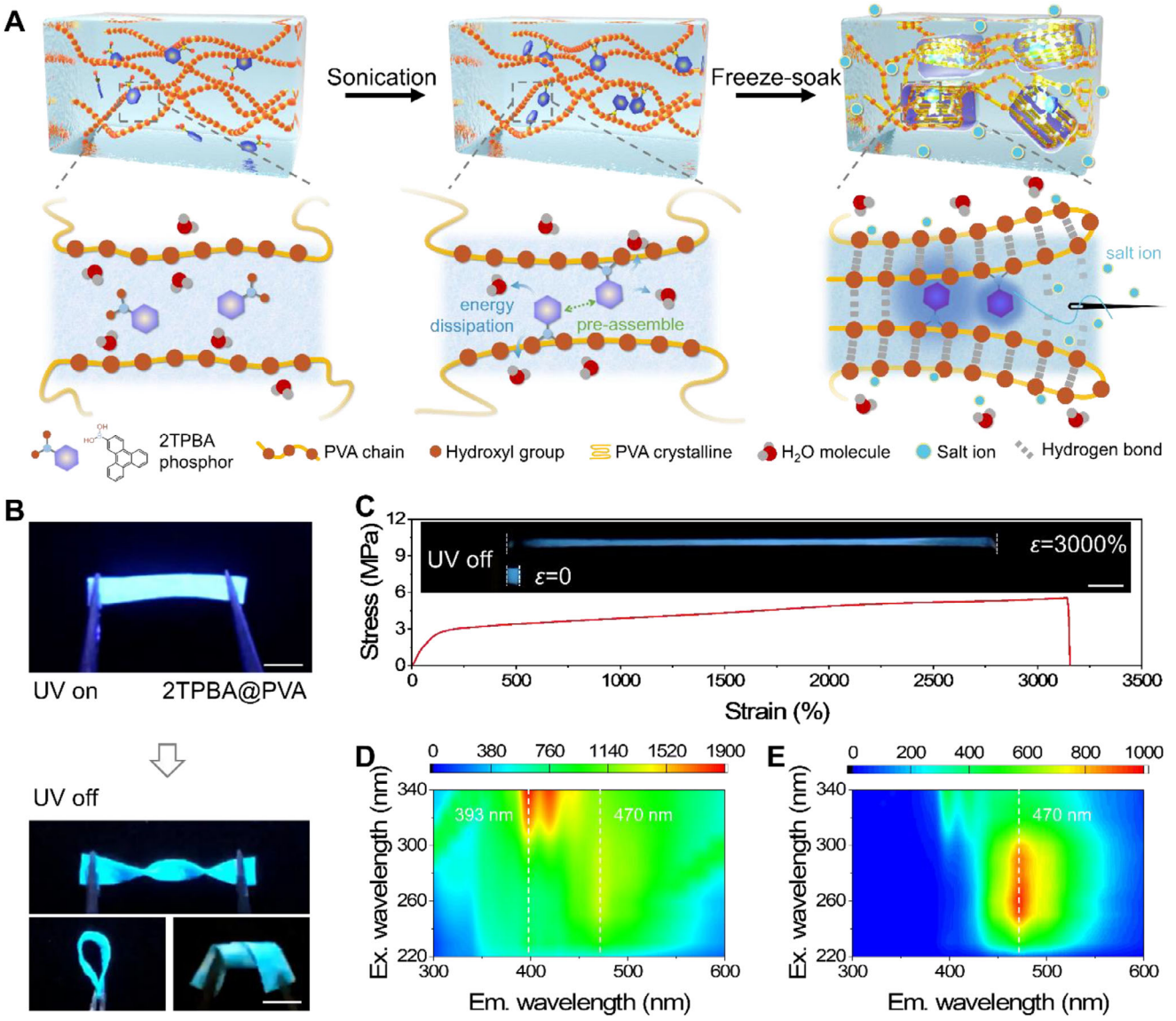

Figure 2. Fabrication of RTPgel. A) Schematic illustration of fabricating RTPgel. B) Images showing an RTPgel going through twisting, bending, and curling without affecting its RTP performance. Scale bar: 5 mm. C) Stretch-strain curve of RTPgel. Inset showing the phosphorescing RTPgel in its original state and stretched to 3000% of its original length, demonstrating exceptional stretchability without loss of phosphorescence. Scale bar: 5 mm. D) Excitation-photoluminescence mapping (no delay) and E) excitation-phosphorescence mapping (delay time = 0.5 ms) of RTPgel. The color change from blue to red indicates the emission intensity.

molecular level, NMR analysis further verifies phosphor-induced chain packing, as the backbone proton signals of 2TPBA-grafted PVA shift upfield relative to pure PVA, indicating reduced interchain spacing (Figure S11, Supporting Information).

The synergy of freeze-thawing and salting-out then plays the most critical role in enhancing phosphorescence as it facilitates the crystallization of PVA chains. As shown in **Figure** 3A,B, both the fluorescence and phosphorescence intensities of the RTPgel increase with longer soaking time (t_{soak}). To quantify the relative enhancement of phosphorescence, we calculated the ratio of phosphorescence intensity at 470 nm to fluorescence intensity at 393 nm (I_{Phos}/I_{Fluo}) from the PL spectra. I_{Phos}/I_{Fluo} got tripled from 0.25 to 0.75 after 24 h of soaking and reached a plateau at 48 h (Figure S12, Supporting Information), indicating the gradual formation and stabilization of the phosphorescent center during the soaking process. Control samples undergoing only the freeze-thaw (F-T gel) or salting-out (S-O gel) procedures were prepared by using the same precursor. To facilitate a parallel comparison of preparation methods, the RTPgel prepared via the freeze–soaking process is also denoted as the F–S gel in this section. Both F-T and S-O gels exhibited weak phosphorescence, with intensities approximately one-tenth of that seen in RTPgel (Figure S13, Supporting Information). The comparison between F-T gel and S-O gel suggests that higher solid content increases phosphorescence due to a greater number of embedded phosphors. However, despite the F-S gel having only half the solid content

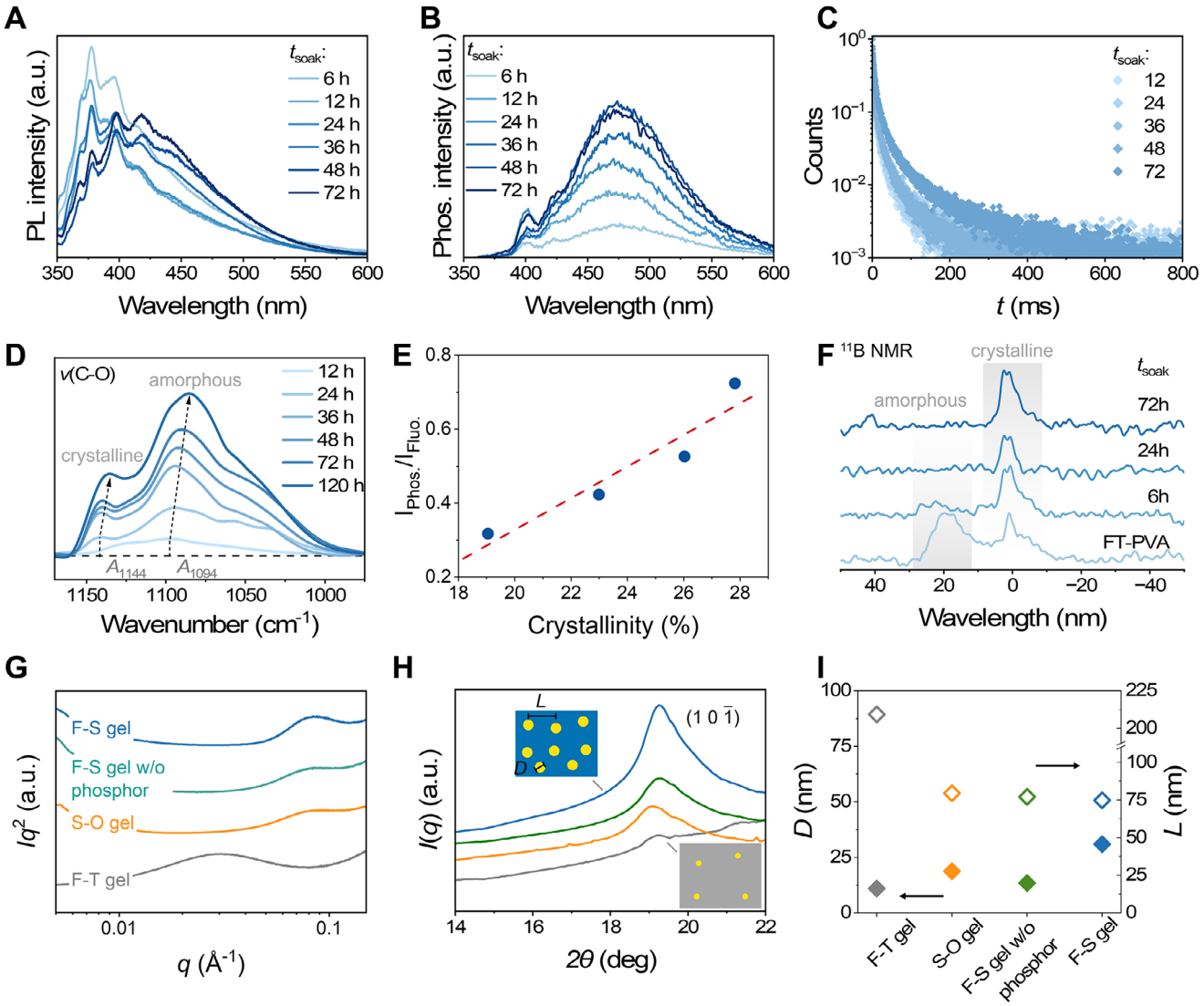

Figure 3. Mechanism of phosphorescence in hydrogel. A) PL spectrum, B) phosphorescence spectrum, and C) phosphorescence lifetime of RTPgels with various soaking times. D) FTIR spectrum of RTPgel with various soaking times. Crystallinity can be calculated from the ratio between the peak area centered 1144 cm^{-1} and 1094 cm^{-1}. E) $I_{Phos.}/I_{Fluo.}$ as a function of hydrogel crystallinity, which shows a positive linear relationship. F) Solid-state ^{11}B NMR spectrum of F-T gel and RTPgel with various soaking times. Representative G) SAXS and H) WAXS profiles of F-T gels, S-O gels, F-S gels without phosphor, and F-S gels. I) Estimated average distance between adjacent crystalline domains L and average crystalline domain size D of F-T gels, S-O gels, F-S gels without phosphor, and F-S gels.

of the S-O gel, its phosphorescence intensity is ten times higher. This indicates that the enhanced phosphorescence in RTPgels results from the unique microenvironment of phosphors formed via the F-S method-triggered PVA assembly. Moreover, although our method also involves freeze-thaw process, results show that it has a negligible contribution compared to the synergy of freeze-thawing and salting-out in terms of provoking phosphorescence, as the number of freeze-thaw cycles has little effect on the phosphorescence property of resulting RTPgel (Figure S14, Supporting Information).

The assembly of PVA chains usually results in the formation of crystalline regions. The crystallinity (α) of RTPgel was acquired by FTIR test (Figure 3D). Peaks located at 1144 and 1094 cm^{-1} are ν(C-O) that existed in the crystalline region and the amorphous region, respectively. The crystallinity can be calculated from the area ratio (A_{1144} / A_{1094}) between these two peaks according to reported equation: $\alpha(\%) = -13.1 + 89.5(A_{1144} / A_{1094})$.[55] As shown in Figure S15 (Supporting Information), the crystallinity of RTPgel steeply increased in the first 48 h of soaking, indicating the shaping of more crystalline regions within the matrix during this period. The relationship of material phosphorescence evolution and crystallinity was summarized in Figure 3E. A linear relationship was observed between I_{Phos}/I_{Fluo} and the crystallinity of PVA, suggesting that the protection provided by PVA microcrystalline domains to embedded phosphors plays a crucial role in stabilizing embedded phosphors and the generation of phosphorescence in a macroscopically soft and wet hydrogel material (Figure S16, Supporting Information).

More direct evidence can be obtained by observing the state of the phosphor. The state of phosphors during the soaking procedure was tracked through solid-state ^{11}B NMR (Figure 3F). Two peaks emerged on the spectrum of freeze-thaw PVA gels with 0 h of soaking, with one broad and located at ~20 ppm, and another one sharp and centered at 0 ppm, corresponding to phosphors that are attached to amorphous chains and crystalline chains, respectively. As the soaking process progressed, the 20 ppm peak gradually diminished, while the 0 ppm peak increased accordingly, suggesting an increasing number of phosphors were trapped in the crystalline region of PVA. After 72 h of soaking, the 20 ppm peak disappeared entirely, suggesting a 100% encapsulation of 2TPBA within the PVA microcrystalline domains. This result supports a model of preferential crystallization around 2TPBA-grafted segments due to preassembly.

To quantify the crystalline morphology and gain a better understanding of the origin of phosphorescence, we measured the inter-domain distance (L) using small-angle X-ray scattering (SAXS) and the crystalline domain size (D) using wide-angle X-ray scattering (WAXS). SAXS measurements were first conducted to obtain the scattering intensity $I(q)$ vs. the scattering vector q (Figure 3G). To accurately identify the peak position, the intensity was corrected by multiplying it by q^2. As shown in Figure 3G, all samples exhibited a clear peak in the corrected Iq^2 versus q plot, indicating the presence of ordered microcrystalline domains. The inter-domain spacing L was calculated using the Bragg equation $L = 2\pi/q_{max}$, where q_{max} is the scattering vector at peak intensity. Among all samples, F-S gels (RTPgel) exhibited the shortest L, indicating the most densely packed crystalline regions compared to F-T gels and S-O gels (Figure 3I).

WAXS measurements were then performed using X-rays with a wavelength of 0.932 Å. As shown in Figure 3H, all samples displayed a noticeable diffraction peak at $2\theta = 19.7°$, corresponding to the characteristic reflection of PVA crystalline planes (101) with an interlayer spacing of 2.7 Å. The average crystalline domain size D was estimated using Scherrer's equation: $D = k\lambda/(\beta\cos\theta)$, where k is the shape factor (taken as 1, assuming approximately spherical domains), λ is the X-ray wavelength, β is the full width at half maximum of the peak, and θ is the Bragg angle. The F-S gels showed a markedly larger domain size (≈30 nm) than F-T (≈11 nm) and S-O gels (≈18 nm), indicating enhanced crystallization (Figure 3I).

Collectively, the F-S gel exhibited both the most densely packed and the largest crystalline regions, correlating strongly with its superior phosphorescence. This confirms the critical role of crystallinity in enabling phosphorescence emission.[41,47] Notably, control F-S gels without phosphor showed smaller D values than S-O gels, highlighting the importance of hydrophobic preassembly in promoting large crystal formation. Two mechanisms may contribute to this: i) the hydrophobic nature of 2TPBA creates a local microenvironment that repels water, facilitating hydrogen bonding between nearby PVA hydroxyl groups; and ii) 2TPBA aggregates act as physical crosslinkers, bringing neighboring chains into closer proximity than those surrounded by water. Consequently, the nucleation of crystalline domains happens preferentially around the phosphors, where molecular motion is strongly suppressed by hydrogen bonding and steric confinement. Meanwhile, the amorphous PVA segments remain hydrated, allowing the gel to retain its macroscopic flexibility and stretchability. Such a mechanism is also supported by the drastic phosphorescence difference between phosphor-doped RTPgel and phosphor-grafted RTPgel, with the former demonstrating significantly weaker phosphorescence and shorter phosphorescence lifetime ≈11.5 ms (Figure S17, Supporting Information). Therefore, the synergistic effect of molecular pre-assembly, freeze-soaking and slating-out is key to forming extensive microcrystalline domains, which underpin the robust phosphorescent behavior of the hydrogel matrix.

Computational simulations were conducted to further elucidate the structural evolution under preassembly, freeze-soaking and salting-out. Molecular dynamics (MD) simulations were performed using a model cell composed of 3 PVA chains (yellow), 20 water molecules (white and red), and 3 sodium citrate (purple), configured according to the experimental ratio. The system was first equilibrated at −5 °C and subsequently evolved at room temperature in the presence of sodium citrate to mimic the freeze-soak (F-S) procedure. The purple shading in Figure S18A (Supporting Information) represents the free volume within the cell. Compared to the pre-soaking state, the post-soaking simulation shows a significant reduction in free volume, attributed to the collapse of PVA chains. Additionally, a decrease in the radius of gyration confirms the compaction of PVA chains, which encapsulates the phosphors and excludes water molecules from the interchain regions (Figure S18B, Supporting Information). As shown in Figure S18C (Supporting Information), the number of hydrogen bonds within the system approximately doubled during the 100 ps simulation, indicating enhanced intermolecular interactions that stabilize the condensed structure.

2.3. RTPgel with Programmable Phosphorescence

According to the Hofmeister series, the type of salt used during the soaking step significantly influences microcrystalline formation and, consequently, the phosphorescent properties of the material. As shown in **Figure** 4C and Movie S4 (Supporting Information), we explored the effects of different salting-out agents, 2 M solutions of sodium acetate (NaAc), sodium sulfate (Na_2SO_4), sodium carbonate (Na_2CO_3), and sodium citrate (Na_3Cit), on the RTP hydrogel. The gel soaked in Na_3Cit exhibited the longest afterglow, lasting up to 8 s. In comparison, gels soaked in Na_2CO_3 and Na_2SO_4 showed afterglows of 8 and 3 s, respectively, while the NaAc-treated gel showed no visible afterglow. Solid-state ^{11}B NMR further confirmed that freeze-soaking in different salting-out solutions enhances phosphor encapsulation by microcrystalline domains compared to freeze-thaw treatment alone. The proportion of encapsulated phosphors relative to the total phosphor content followed the trend: NaAc < Na_2CO_3 < Na_2SO_4 < Na_3Cit. This trend directly correlates with the phosphorescence performance of the corresponding hydrogels, supporting the proposed mechanism of microcrystalline protection. Moreover, it aligns precisely with the Hofmeister series, indicating that the phosphorescent behavior of RTPgels can be effectively tuned by salt selection, offering a precisely programmable approach to control their luminescence characteristics. Salting-in salts such as NaCl, $NaNO_3$, and NaI were also adopted to soak the hydrogel. No phosphorescence was observed in hydrogels soaked in NaCl

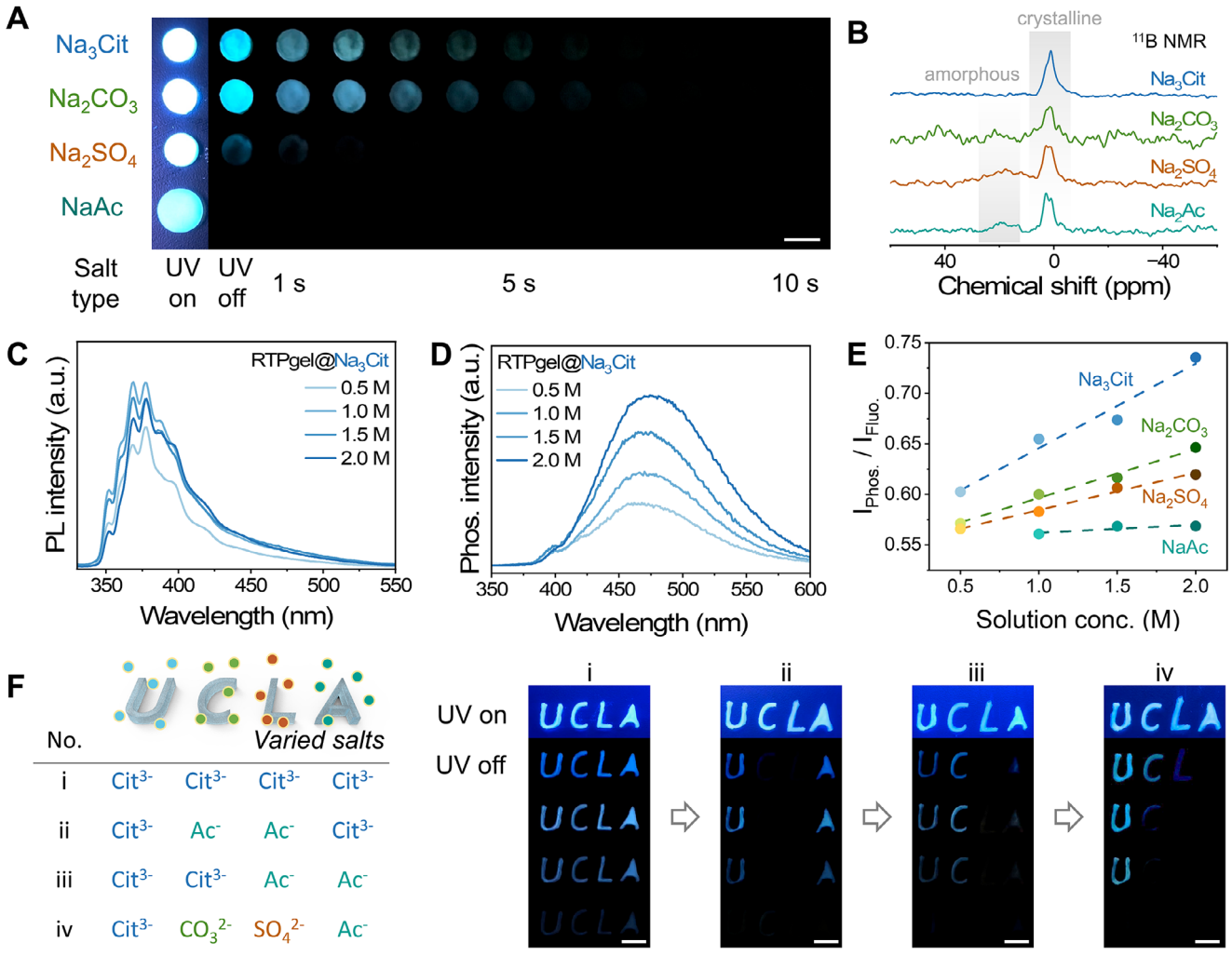

Figure 4. Tailoring the emission properties of RTPgels. A) Images showing the afterglow of RTPgels soaked in various salt solutions (1 M). Scale bar: 5 mm. B) ^{11}B NMR spectrum of RTPgels soaked in various salt solutions. C) PL spectrum and D) phosphorescence spectrum of RTPgel soaked in Na_3Cit solutions with various concentrations. E) $I_{Phos.}/I_{Fluo.}$ as a function of salt solution concentration of various salts. F) Spatiotemporal programming of the phosphorescence properties of RTPgel for diverse patterns by soaking in various kinds of salt solutions. Excitation wavelength: 365 nm. Scale bar: 5 mm.

or $NaNO_3$ solutions, while the hydrogel dissolved completely in NaI solution (Figure S19, Supporting Information).

Salt concentration regulates the ionic strength of the solution, which directly influences polymer assembly behavior, making it an effective parameter for tailoring phosphorescence properties (Figure S20, Movie S5, Supporting Information). Taking sodium citrate (Na_3Cit) as an example, its fluorescence intensity peaked at 1.0 M, then gradually declined at higher concentrations (1.5 M and 2.0 M), when, in contrast, phosphorescence intensity continued to increase with rising Na_3Cit concentration. Furthermore, the sensitivity of phosphorescence to salt concentration reflects the Hofmeister series. As shown in Figure 4D, the I_{Phos}/I_{Fluo} ratio varies significantly with salt concentration, depending on the salt type. The RTPgel treated with Na_3Cit exhibited the steepest change, with a slope of 0.083, followed by Na_2CO_3 (0.048) and Na_2SO_4 (0.036). NaAc showed minimal sensitivity, with a nearly flat slope of 0.0037. These results highlight the crucial role of both the type and concentration of salt in programming the phosphorescent response of RTPgels.

Since both salt type and concentration significantly influence RTP, they can be effectively used to program the phosphorescence behavior of RTPgels. Cyclic soaking of RTPgels in different salt solutions results in corresponding changes in phosphorescence intensity and lifetime (Figures S21 and S22, Supporting Information). Representative demonstrations are shown in Figure 4F, where RTPgels shaped into the letters "U," "C," "L," and "A" were treated to display various afterglow lifetimes. Initially, all four letter-shaped gels were soaked in sodium citrate solution, giving them identical RTP lifetimes. As a result, the entire "UCLA" pattern exhibited uniform afterglow that faded simultaneously upon removal of excitation light (Figure 4F-i; Movie S6, Supporting Information). In the next step, the "C" and "L" gels were soaked in sodium acetate for 24 h. After this treatment, only the "U" and "A" gels

retained obvious afterglow, while the "C" and "L" gels lost their afterglow immediately after the excitation light was turned off, effectively transforming the visible pattern from "UCLA" to "UA" (Figure 4F-ii). Subsequently, the phosphorescent display was reprogrammed by soaking the "C" gel again with sodium citrate, while the "A" gel was treated with sodium acetate (Figure 4F-iii). This adjustment altered the visible pattern to "UC". Spatiotemporal displays were also achieved by soaking each letter in a distinct salt solution, citrate, sulfate, chloride, and acetate for "U", "C", "L", and "A", respectively, resulting in a time-resolved fading sequence: "UCLA" → "UCL" → "UC" → "U" (Figure 4F-iv). A similar effect was obtained by treating all RTPgels with the same salt type (Na_3Cit) but at varying concentrations (Figure S23, Supporting Information). This simple soaking-programming strategy offers a robust and flexible platform for creating programmable phosphorescent materials, with broad potential applications in anti-counterfeiting, information encoding/storage, and intelligent visual signaling.[40,56]

2.4. Multi-Color Afterglow Hydrogels (MCA gel)

Color coverage is another key property of luminescent material. Multi-color afterglow (MCA) could be feasibly achieved by freeze-soaking the RTPgels precursor, which was mixed with different commercial dyes. Specifically, according to the phosphorescence resonance energy transfer (PRET) effect, specific dyes can serve as acceptors when the 2TPBA phosphor within the RTPgel matrix serves as donors, for luminescence after turning off the excitation source through consistent triplet-to-singlet energy transfer (**Figure 5**A,B).[49,57,58] Fluorescein sodium (Fluo S), rhodamine 6G (Rhod 6G), and rhodamine B (Rhod B) were selected as possible acceptors due to the partial overlap between their absorbance spectra with the phosphorescence spectrum of RTP PVA (Figure 5C). Fluorescent dyes (Fluo S) were first mixed with the RTPgel precursor at specific ratios and then subjected to the freeze-soak process to fabricate multi-color afterglow hydrogels (FS-MCAgels). As a control, another set of MCAgels was prepared by soaking pre-formed RTPgels in salt solutions containing Fluo S, thereby introducing the dyes via post-doping (referred to as doping-MCAgels). These two fabrication routes led to MCAgels with markedly different phosphorescent properties. In the FS-MCAgels, mixing the dyes with the precursor prior to freeze-soaking allows the dyes to be co-confined within the microcrystalline regions and positioned in close proximity to the phosphors. This spatial arrangement enhances donor-to-acceptor energy transfer. In contrast, when dyes are introduced after the freeze-soaking step, they remain in the aqueous phase, while only the phosphors are embedded in the crystalline domains. This separation limits energy transfer due to the increased spatial distance and the presence of water molecules that can dissipate energy rather than facilitate transfer (Figure 5D). As a result, FS-MCAgels exhibit significantly stronger phosphorescence and longer lifetimes compared to doping-MCAgels (Figures 5E; S24, Supporting Information), further validating the effectiveness of the proposed freeze-soak strategy for fabricating high-performance RTP hydrogels.

As shown in Figure 5F and Movie S7 (Supporting Information), FS-MCAgels that contains Fluo S, Rhod 6G and Rhod B enlarge the stokes shift between excitation source (305 nm) and phosphorescent peak of 2TPBA (455 nm, blue), redshift the central afterglow peak to 547 nm (green), 574 nm (yellow) and 604 nm (red), respectively. MCA gels with the doping ratio at 0.05 wt% (weight ratio to PVA) have the longest afterglow lasting for ~ 8 s (Figure S25, Supporting Information). PRET efficiency (Φ_{FRET}) was calculated to be 75%, 81%, 59% for MCA gel doped with 0.05 wt% Fluo S (G), Rhod 6G (Y) and Rhod B (R), respectively (Figure 5C,D, Table S1, Supporting Information, $\Phi_{FRET} = 1\text{-}\tau_D/\tau_{D,0}$, where τ_D and $\tau_{D,0}$ are the RTP lifetimes of energy donor before and after energy transfer),[59] suggesting the strong potential of the PRET strategy in achieving long-lasting multi-color after glow. Increasing the doping amount of dye would lead to decreased afterglow time, possibly due to the self-absorption effect of free dyes that dissolved in water. Elaborating on the synergetic emission of multiple dyes, an afterglow that covers the full spectrum can be achieved. As shown in Figure 5D and Movie S8 (Supporting Information), afterglow color falls into green-to-yellow, yellow-to-red afterglow colors have been achieved by co-doping Fluo S & Rhod 6G, and Rhod B, respectively.

2.5. Material and Processing Universality

Our F-S method for fabricating hydrogel-based RTP materials demonstrates broad universality and can be extended to a variety of phosphors and polymer matrices. To showcase this versatility, a series of borate-based phosphors, 4-dibenzothienylboronic acid (DBTBA, 1), 1, 3, 5-tris[(4-phenylboronic acid)]benzene (TPBBA, 2), 2-naphthaleneboronic acid (2NBA, 3), 1, 1′-binaphthyl-4-ylboronic acid (BNBA, 4), fluoranthene-3-boronic acid (FLBA, 5), featuring diverse conjugated aromatic moieties were used to construct phosphorescent hydrogels (**Figure 6**A). The resulting hydrogels exhibit distinct dominant emission peaks centered at 497, 511, 523, 537, and 550 nm, respectively, highlighting the potential of the F-S method for producing multi-color phosphorescent hydrogels with finely tunable luminescent properties (Figures 6B; S26 and Movie S9, Supporting Information). Moreover, all these hydrogels displayed long phosphorescent lifetimes (Figure 6C; Table S2, Supporting Information), confirming the general effectiveness of the F-S strategy across different phosphor systems. In addition to PVA, other polymers such as gelatin and collagen also proved compatible with the F-S method. As illustrated in Figure 6D, gelatin- and collagen-based hydrogels grafted with 2TPBA phosphor exhibited obvious afterglow. This phosphor and polymer versatility enables not only the fabrication of multi-color RTP hydrogels but also provides flexibility in material selection tailored for specific applications, including in vivo bioimaging, chemical tracing, and environmental monitoring.

Beyond the universality in matrix and phosphor selection, the F-S method is highly adaptable to a wide range of advanced processing technologies, allowing for material shaping and casting on demand.[8,60,61] For instance, the PVA-based precursor can be readily extruded through nozzles to form hydrogel fibers. As shown in Figure 6E, MCAgel fibers in red, yellow, green, and blue were fabricated on a large scale (up to 5 meters each) via a combined extrusion and F-S process. Direct

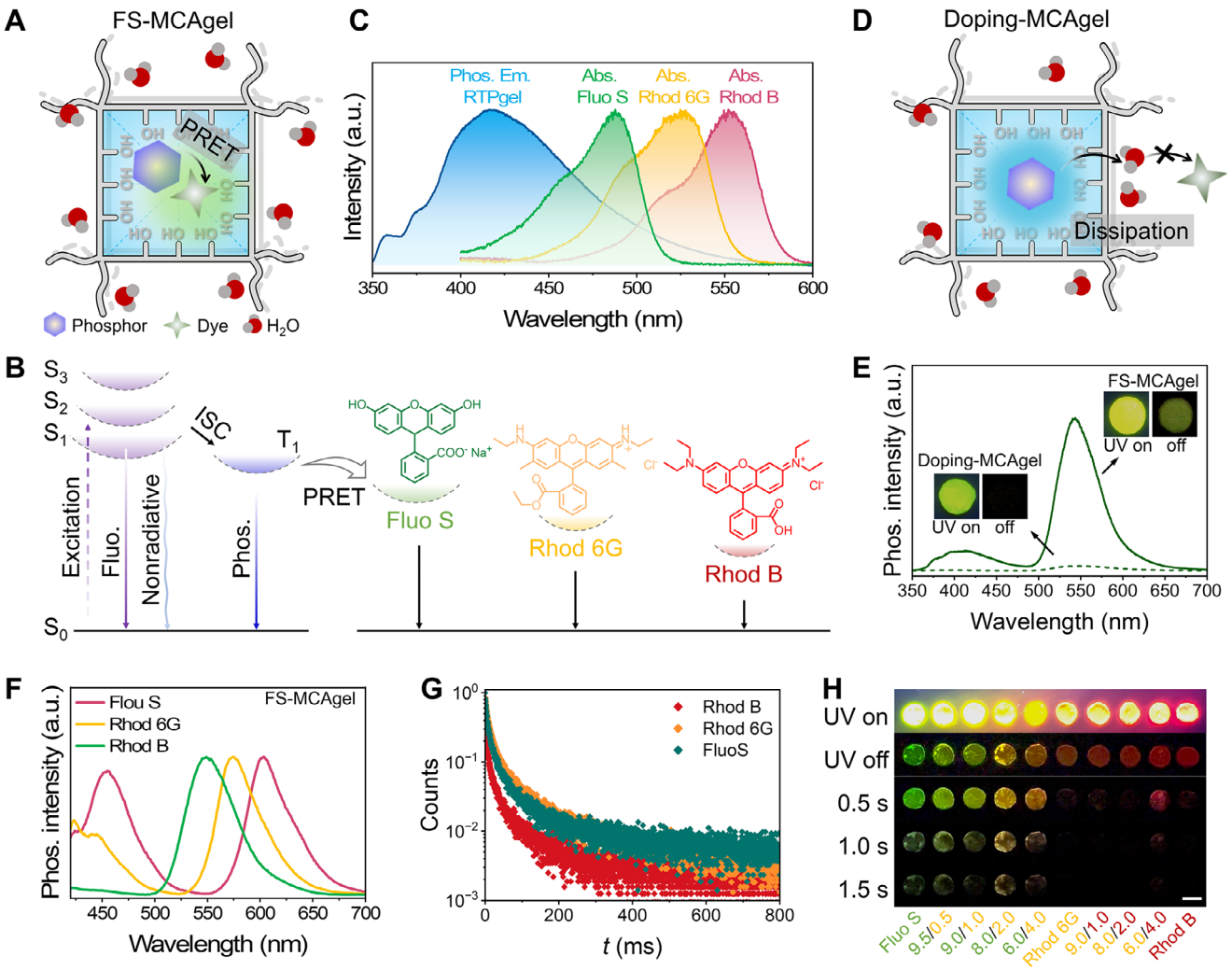

Figure 5. Multicolor afterglow (MCA) achieved by freeze-soak RTPgel precursor doped with various dyes. A,B) Schematic illustration of phosphorescence resonance energy transfer (PRET) from the T_1 state of FS-RTPgel to various dyes for multicolor afterglow. C) Phosphorescence emission spectrum of RTPgel overlapping the absorbance spectrum of various commercial dyes. D) Schematic illustration of the ineffective D-A energy transfer in gels made by doping dyes into RTPgels (doping-MCAgel). E) Delayed luminescence spectrum of FS-MCAgel and Doping-MCAgel. F) Delayed luminescence spectrum showing the multicolor afterglow of RTPgels doped with various dyes. G) Afterglow lifetime of MCAgels. H) Image of FS-MCAgel with wide color coverage. Excitation wavelength: 365 nm. Scale bar: 5 mm.

ink writing (DIW), another extrusion-based technique, offers a versatile route for customizing RTPgels. A printable ink composed of gelatin and 2TPBA@PVA (10 wt%, 1:1 w/w) was formulated, which remained extrudable at elevated temperatures (60 °C) and rapidly gelated upon cooling to room temperature (Figure S27, Supporting Information). This approach enabled the creation of RTP hydrogels with customizable 3D complex geometries, such as the hollow cylindrical structures depicted in Figure 6F.

For higher-resolution patterning, digital light processing (DLP) was employed. A photo-curable system was formulated by blending acrylamide, initiator, and crosslinker with the RTPgel precursor. The mixture was coated onto glass substrates and exposed to patterned light using a reflective setup with a projector (Figure 6G).[62] Multicolor phosphorescent patterns spelling "*RTP GEL*" were successfully fabricated on a centimeter scale. High-resolution patterns with more than 80 words also became printable within a tiny area as large as a coin, demonstrating the exceptional processing flexibility of our method for fabricating gel-state phosphorescent materials with precise control.

3. Conclusion

Hydrogel materials rarely exhibit RTP due to their soft and hydrated nature, which limits their potential in advanced optical applications. In this work, we proposed a novel strategy to fabricate RTP hydrogels by leveraging the synergy of freeze-soaking and salting-out. The resulting RTPgels exhibit lifetimes >200 ms and long-lasting afterglow (>10 s), while maintaining high hydration (≈71%) and flexibility (>3000%). The phosphorescence is easily tunable by re-soaking the hydrogels with

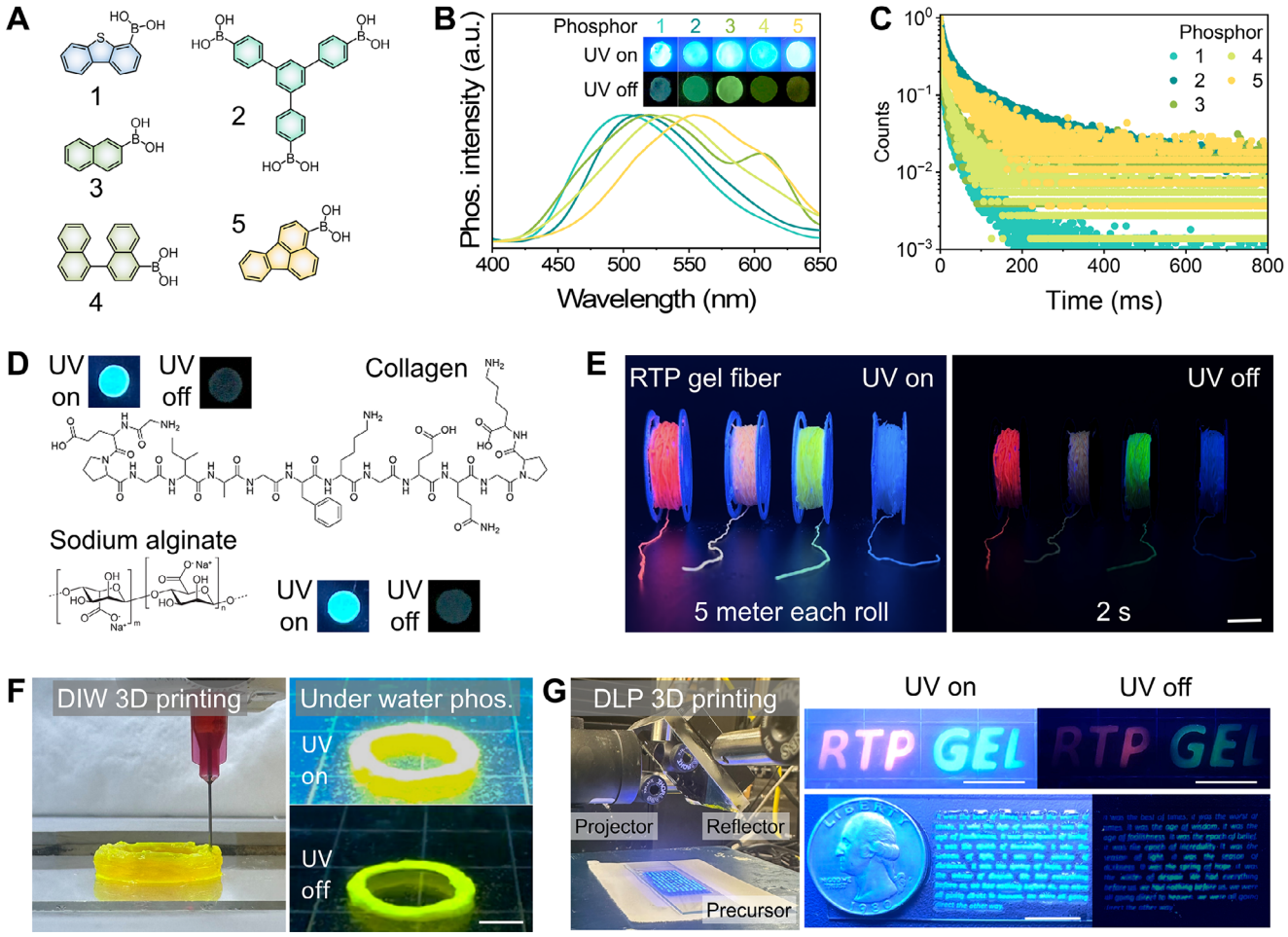

Figure 6. Material and processing universality of the freeze-soak method for RTPgels. A) Representative boronic acid-based phosphors, including DBTBA (1), TPBBA (2), 2NBA (3), BNBA (4), and FLBA (5), that are adaptable for creating RTPgels. B) Phosphorescence spectrum and C) phosphorescence lifetime of RTPgels made from phosphor 1-5. D) RTPgels made from collagen and sodium alginate as the polymer matrix. E) Image of multicolor RTP hydrogel fibers when UV light was on and turned off for 2 s. Scale bar: 10 mm F) DIW 3D printing of RTPgel with 2TPBA@PVA/gelatin ink. Printed hydrogel ring demonstrated long-lasting afterglow under water. Scale bar: 5 mm. G) Multicolor DLP 3D printing of RTPgel pattern with high precision. Scale bar: 10 mm.

different salt solutions or concentrations, enabling the creation of programmable spatiotemporal emission patterns, which is highly promising for advanced anti-counterfeiting systems. A key advantage of the F-S approach is its broad universality. It accommodates diverse boronic acid-based luminophores and functions across multiple polymer matrices, including biopolymers. Equally important, the method is inherently scalable and compatible with a wide range of fabrication techniques, such as fiber spinning, direct ink writing, and DLP-based printing, which allows RTP hydrogels to be produced in customized geometries and at various length scales without altering the underlying chemistry. We also recognize that although this strategy imparts strong RTP performance and mechanical robustness, the high residual ion content and susceptibility to dehydration remain key challenges for practical use. These issues may restrict direct biomedical applications and limit long-term environmental stability. Future work will aim to address these limitations by introducing biocompatible salts and developing water-retentive or encapsulated designs to enhance durability.[63,64,65]

Overall, this efficient and versatile strategy provides a robust platform for creating tough phosphorescent hydrogels with broad potential in chemical sensing, soft actuation, soft electronics, and anti-counterfeiting.

Supporting Information

Supporting Information is available from the Wiley Online Library or from the author.

Acknowledgements

M.S. and W.F. contributed equally to this work. This research was performed on APS beam time award (DOI: https://doi.org/10.46936/APS-189597/60013778) from the Advanced Photon Source, a U.S. Department of Energy (DOE) Office of Science user facility operated for the DOE Office of Science by Argonne National Laboratory under Contract No. DE-AC02-06CH11357. Wei Lu and Tao Chen thank the support from the Natural Science Foundation of China (22322508), Zhejiang Provincial Natural Science Foundation of China (LR23E030001).

Conflict of Interest

The authors declare no conflict of interest.

Data Availability Statement

The data that support the findings of this study are available from the corresponding author upon reasonable request.

Keywords

3D printing, flexible phosphorescent material, hoffmeister effect, luminescent hydrogel, room temperature phosphorescence

Received: September 22, 2025
Revised: November 21, 2025
Published online:

[1] W. J. Zhao, Z. K. He, B. Z. Tang, *Nat. Rev. Mater.* **2020**, *5*, 869.
[2] G. Yin, J. Zhou, W. Lu, L. Li, D. Liu, M. Qi, B. Z. Tang, P. Theato, T. Chen, *Adv. Mater.* **2024**, *36*, 2311347.
[3] Y. Yang, A. Li, Y. Yang, J. Wang, Y. Chen, K. Yang, B. Z. Tang, Z. Li, *Angew. Chem., Int. Ed.* **2023**, *62*, 202308848.
[4] X. Wei, C. Zhang, S. He, J. Huang, J. Huang, S. S. Liew, Z. Zeng, K. Pu, *Angew. Chem., Int. Ed.* **2022**, *61*, 202202966.
[5] Z. Zeng, S. S. Liew, X. Wei, K. Pu, *Angew. Chem., Int. Ed.* **2021**, *60*, 26454.
[6] J. Yin, P. Jia, Z. Ren, Q. Zhang, W. Lu, Q. Yao, M. Deng, X. Zhou, Y. Gao, N. Liu, *Adv. Mater.* **2025**, *37*, 2417944.
[7] J. Yin, P. Jia, Z. Ren, Q. Zhang, W. Lu, Q. Yao, M. Deng, X. Zhou, Y. Gao, N. Liu, *Research* **2025**, *8*, 0571.
[8] L. Li, D. Liu, J. Zhou, M. Qi, G. Yin, T. Chen, *Mater. Horiz.* **2024**, *11*, 5895.
[9] K. Zhang, L. Y. Peng, X. X. Liu, X. Xu, W. H. Fang, G. Cui, Y. Z. Chen, C. H. Tung, L. Z. Wu, *Angew. Chem., Int. Ed.* **2023**, *62*, 202300927.
[10] Z. Xie, X. Zhang, H. Wang, C. Huang, H. Sun, M. Dong, L. Ji, Z. An, T. Yu, W. Huang, *Nat. Commun.* **2021**, *12*, 3522.
[11] D. Li, F. Lu, J. Wang, W. Hu, X. M. Cao, X. Ma, H. Tian, *J. Am. Chem. Soc.* **2018**, *140*, 1916.
[12] H. J. Yu, Q. Zhou, X. Dai, F. F. Shen, Y. M. Zhang, X. Xu, Y. Liu, *J. Am. Chem. Soc.* **2021**, *143*, 13887.
[13] W. Feng, F. Li, Z. Jiang, C. Yue, G. Yin, N. Zhu, K. Zhang, T. Chen, W. Lu, *Angew. Chem., Int. Ed.* **2025**, *137*, 202505192.
[14] Y. Zhang, Y. Su, H. Wu, Z. Wang, C. Wang, Y. Zheng, X. Zheng, L. Gao, Q. Zhou, Y. Yang, X. Chen, C. Yang, Y. Zhao, *J. Am. Chem. Soc.* **2021**, *143*, 13675.
[15] L. Ma, S. Sun, B. Ding, X. Ma, H. Tian, *Adv. Funct. Mater.* **2021**, *31*, 2010659.
[16] X. W. Liu, W. Zhao, Y. Wu, Z. Meng, Z. He, X. Qi, Y. Ren, Z. Q. Yu, B. Z. Tang, *Nat. Commun.* **2022**, *13*, 3887.
[17] X. P. Zhang, J. K. Liu, B. A. Chen, X. W. He, X. Y. Li, P. F. Wei, P. F. Gao, G. Q. Zhang, J. W. Y. Lam, B. Z. Tang, *Matter* **2022**, *5*, 3499.
[18] H. Ju, H. Zhang, L. X. Hou, M. Zuo, M. Du, F. Huang, Q. Zheng, Z. L. Wu, *J. Am. Chem. Soc.* **2023**, *145*, 3763.
[19] J. Ren, Y. Wang, Y. Tian, Z. Liu, X. Xiao, J. Yang, M. Fang, Z. Li, *Angew. Chem., Int. Ed.* **2021**, *60*, 12335.
[20] M. Qi, J. Huang, J. Wei, J. Zhou, D. Liu, L. Li, W. Luo, G. Yin, T. Chen, *Angew. Chem., Int. Ed.* **2025**, *64*, 202501054.
[21] Y. Ren, W. Dai, S. Guo, L. Dong, S. Huang, J. Shi, B. Tong, N. Hao, L. Li, Z. Cai, Y. Dong, *J. Am. Chem. Soc.* **2022**, *144*, 1361.
[22] H. Liu, W. Ye, Y. Mu, H. Ma, A. Lv, S. Han, H. Shi, J. Li, Z. An, G. Wang, W. Huang, *Adv. Mater.* **2022**, *34*, 2107612.
[23] B. Zhou, Z. Qi, D. Yan, *Angew. Chem., Int. Ed.* **2022**, *61*, 202208735.
[24] B. Zhou, G. Xiao, D. Yan, *Adv. Mater.* **2021**, *33*, 2007571.
[25] K. Chen, Y. Zhang, Y. Lei, W. Dai, M. Liu, Z. Cai, H. Wu, X. Huang, X. Ma, *Nat. Commun.* **2024**, *15*, 1269.
[26] S. Cai, Z. Sun, H. Wang, X. Yao, H. Ma, W. Jia, S. Wang, Z. Li, H. Shi, Z. An, Y. Ishida, T. Aida, W. Huang, *J. Am. Chem. Soc.* **2021**, *143*, 16256.
[27] W. Ye, H. Ma, H. Shi, H. Wang, A. Lv, L. Bian, M. Zhang, C. Ma, K. Ling, M. Gu, Y. Mao, X. Yao, C. Gao, K. Shen, W. Jia, J. Zhi, S. Cai, Z. Song, J. Li, Y. Zhang, S. Lu, K. Liu, C. Dong, Q. Wang, Y. Zhou, W. Yao, Y. Zhang, H. Zhang, Z. Zhang, X. Hang, et al., *Nat. Mater.* **2021**, *20*, 1539.
[28] H. Liu, C. Du, L. Liao, H. Zhang, H. Zhou, W. Zhou, T. Ren, Z. Sun, Y. Lu, Z. Nie, F. Xu, J. Zhu, W. Huang, *Nat. Commun.* **2022**, *13*, 3420.
[29] Y. Zhang, L. Gao, X. Zheng, Z. Wang, C. Yang, H. Tang, L. Qu, Y. Li, Y. Zhao, *Nat. Commun.* **2021**, *12*, 2297.
[30] D. Li, J. Yang, M. Fang, B. Z. Tang, Z. Li, *Sci. Adv.* **2022**, *8*, abl8392.
[31] Y. Yu, M. Q. Si, W. Lu, S. S. Wu, S. X. Wei, B. Y. Wu, X. P. Chen, W. P. Xie, T. Chen, *Chem. Eng. J.* **2023**, *478*, 147271.
[32] J. Deng, D. Liu, H. Liu, L. Yu, Y. Bai, J. Xiao, H. Wang, *Adv. Funct. Mater.* **2024**, *34*, 2408821.
[33] J. Deng, H. Liu, D. Liu, L. Yu, Y. Bai, W. Xie, T. Li, C. Wang, Y. Lian, H. Wang, *Adv. Funct. Mater.* **2023**, *34*, 2308420.
[34] Y. Cao, D. Wang, Y. Zhang, G. Li, C. Gao, W. Li, X. Chen, X. Chen, P. Sun, Y. Dong, Z. Cai, Z. He, *Angew. Chem., Int. Ed.* **2024**, *63*, 202401331.
[35] H. Chen, X. Ma, S. Wu, H. Tian, *Angew. Chem., Int. Ed.* **2014**, *53*, 14149.
[36] X. Fan, L. Gao, Y. Jin, T. Qiu, X. Banquy, X. X. Zhu, C. Zhao, *Adv. Opt. Mater.* **2024**, *13*, 2402627.
[37] S. Tang, S. Jiang, K. Wang, Y. Zhang, L. Yi, J. Hou, L. Qu, Y. Zhao, C. Yang, *Adv. Mater.* **2025**, *37*, 2416397.
[38] W. Luo, L. Chen, G. Yin, C. Yue, S. Xie, J. Zhou, W. Feng, Y. Nie, H. Qiu, F. Li, S. Cai, Y. Li, Z. Cai, T. Chen, *Angew. Chem., Int. Ed.* **2025**, *137*, 202423650.
[39] L. Li, J. Zhou, J. Han, D. Liu, M. Qi, J. Xu, G. Yin, T. Chen, *Nat. Commun.* **2024**, *15*, 3846.
[40] Y. Dong, S. Feng, W. Huang, X. Ma, *Chem. Soc. Rev.* **2025**, *54*, 3681.
[41] S. Wu, M. Hua, Y. Alsaid, Y. Du, Y. Ma, Y. Zhao, C. Y. Lo, C. Wang, D. Wu, B. Yao, J. Strzalka, H. Zhou, X. Zhu, X. He, *Adv. Mater.* **2021**, *33*, 2007829.
[42] B. A. Deyerle, Y. Zhang, *Langmuir* **2011**, *27*, 9203.
[43] F. Al-Sagheer, M. J. Hey, *Colloids Surf., A* **2004**, *245*, 99.
[44] C. Yin, Z. Huang, Y. Zhang, K. Ren, S. Liu, H. Luo, Q. Zhang, Y. Wan, *J. Mater. Chem. B* **2024**, *12*, 3079.
[45] J. Li, H. L. Chee, Y. T. Chong, B. Q. Y. Chan, K. Xue, P. C. Lim, X. J. Loh, F. Wang, *ACS Appl. Mater. Interfaces* **2022**, *14*, 23826.
[46] C. Zeng, P. Wu, J. Guo, N. Zhao, C. Ke, G. Liu, F. Zhou, W. Liu, *Soft Matter* **2022**, *18*, 8675.
[47] M. Hua, S. Wu, Y. Ma, Y. Zhao, Z. Chen, I. Frenkel, J. Strzalka, H. Zhou, X. Zhu, X. He, *Nature* **2021**, *590*, 594.
[48] Y. J. Jin, S. Lu, X. R. Chen, Q. Y. Fang, X. Guan, L. G. Qin, C. Y. Chen, C. Z. Zhao, *Macromolecules* **2024**, *57*, 2746.
[49] W. G. Chen, Y. Wang, Z. J. Chen, H. J. Wei, L. Dang, Z. Z. Lin, Y. Chen, Y. Wang, *Adv. Opt. Mater.* **2023**, *12*, 2302424.
[50] F. Nie, D. Yan, *Angew. Chem., Int. Ed.* **2023**, *62*, 202302751.
[51] Y. Zhang, X. Chen, J. Xu, Q. Zhang, L. Gao, Z. Wang, L. Qu, K. Wang, Y. Li, Z. Cai, Y. Zhao, C. Yang, *J. Am. Chem. Soc.* **2022**, *144*, 6107.
[52] J. Wei, C. Liu, J. Duan, A. Shao, J. Li, J. Li, W. Gu, Z. Li, S. Liu, Y. Ma, W. Huang, Q. Zhao, *Nat. Commun.* **2023**, *14*, 627.
[53] J. You, X. Zhang, Q. Nan, K. Jin, J. Zhang, Y. Wang, C. Yin, Z. Yang, J. Zhang, *Nat. Commun.* **2023**, *14*, 4163.
[54] S. Q. Ma, S. J. Du, G. C. Pan, S. T. Dai, B. Xu, W. J. Tian, *Aggregate* **2021**, *2*, 96.
[55] O. N. Tretinnikov, S. A. Zagorskaya, *J. Appl. Spectrosc.* **2012**, *79*, 521.

[56] J. Y. Zhou, D. P. Liu, L. Q. Li, M. Qi, G. Q. Yin, T. Chen, *Chin. Chem. Lett.* **2024**, *35*, 109929.
[57] X. Zhang, M. Zeng, Y. Zhang, C. Zhang, Z. Gao, F. He, X. Xue, H. Li, P. Li, G. Xie, H. Li, X. Zhang, N. Guo, H. Cheng, A. Luo, W. Zhao, Y. Zhang, Y. Tao, R. Chen, W. Huang, *Nat. Commun.* **2023**, *14*, 475.
[58] X. Y. Dai, M. Huo, Y. Liu, *Nat. Rev. Chem.* **2023**, *7*, 854.
[59] X. Yu, K. Liu, B. Wang, H. Zhang, Y. Qi, J. Yu, *Adv. Mater.* **2023**, *35*, 2208735.
[60] Y. Miao, F. Lin, D. Guo, J. Chen, K. Zhang, T. Wu, H. Huang, Z. Chi, Z. Yang, *Sci. Adv.* **2024**, *10*, adk3354.
[61] G. Yin, W. Lu, J. Huang, R. Li, D. Liu, L. Li, R. Zhou, G. Huo, T. Chen, *Aggregate* **2023**, *4*, 344.
[62] M. Hua, D. Wu, S. Wu, Y. Ma, Y. Alsaid, X. He, *ACS Appl. Mater. Interfaces* **2021**, *13*, 12689.
[63] H. Yuk, T. Zhang, G. A. Parada, X. Liu, X. Zhao, *Nat. Commun.* **2016**, *7*, 12028.
[64] H. Yuan, T. Zhu, Y. Huang, Z. Wang, P. Han, L. Tan, J. Wu, X. Chen, P. Yao, C. Zhu, J. Xu, *Adv. Funct. Mater.* **2024**, *34*, 2409703.
[65] F. Ni, P. Xiao, C. Zhang, T. Chen, *Matter* **2022**, *5*, 2624.